

Laser-cluster interaction with subcycle pulses

M. Kundu,¹ P. K. Kaw,¹ and D. Bauer²

¹*Institute for Plasma Research, Bhat, Gandhinagar, Gujarat-382 428, India*

²*Institut für Physik, Universität Rostock, 18051 Rostock, Germany*

(Received 22 September 2011; published 29 February 2012)

The interaction of intense laser light with atomic nanoclusters is studied with a rigid sphere model and three-dimensional particle-in-cell simulations for ultrashort laser pulses of pulse durations τ down to one optical period T and below. In this subcycle regime not all conventional pulse models are applicable and may lead to unphysical absorption of laser energy. For allowed pulse models, we show that for a given laser peak intensity, and cluster, the efficiency of laser absorption increases as τ shortens and reaches a maximum value in the subcycle regime. For deuterium clusters, where inner ionization quickly saturates, the absorbed energy and outer ionization reaches a peak at $\tau \approx 0.8T$. For argon clusters, however, such a peak disappears, and energy absorption continues even for $\tau < 0.8T$ due to additional inner ionization.

DOI: [10.1103/PhysRevA.85.023202](https://doi.org/10.1103/PhysRevA.85.023202)

PACS number(s): 36.40.Gk, 52.25.Os, 52.50.Jm, 42.65.Re

I. INTRODUCTION

Laser-based, table-top, particle (electrons, ions), and light sources (x rays) require efficient coupling of laser energy to matter. Nanoclusters formed in an atomic gas jet were shown to be an efficient absorber of laser light. With the cluster size being much smaller than the wavelength λ (usually 248–1064 nm), the laser radiation can efficiently couple to the solidlike atomic density with negligible skin-layer reflection and without hot electrons escaping into a cold bulk. Because of these advantages nearly 90% of laser energy can be absorbed [1] in clusters, producing ions of near MeV energies [1–8], electrons with keV energies [9–13], harmonic radiation [14–18], and x rays [19–22]. Nuclear fusion was also demonstrated with laser-heated deuterium clusters [23].

Experimentally, laser-cluster interaction is commonly studied with a pump-probe setup [24] (also see Refs. [25,26] for review). The pump laser of frequency ω first ionizes the cluster, leading to a prompt increase of the charge density $\rho(t)$ as well as the Mie-plasma frequency $\omega_M(t) = \omega_p/\sqrt{3} = \sqrt{4\pi\rho(t)/3} > \omega$ (ω_p is the plasma frequency, atomic units $|e| = m = 4\pi\epsilon_0 = 1$ are used unless mentioned explicitly). Subsequent displacement of the electrons from the quasistatic ion background leads to a space charge field, which may exceed the applied laser field. The total field (space charge plus laser field) may cause further ionization of ions, known as ionization ignition [27–32]. This ionization ignition and ionization of atoms/ions (inner ionization) depends upon the number of electrons leaving the cluster as a whole, called outer ionization. Outer ionization leaves behind a net positively charged ionic background, which later explodes due to Coulomb repulsion. During the expansion, enhanced energy absorption may take place when $\omega_M(t) = \omega$ is met at a later time, typically >50 fs [24] for 800 nm laser, provided the laser pulse is long enough. This linear resonance (LR) has been studied within a nanoplasma model [33] where the expanding cluster was assumed to be homogeneously charged. However, in reality, ions near the cluster boundary are disintegrated and leave the cluster with higher kinetic energy much earlier than the relatively slow ions in the cluster core. Only in the nearly homogeneous core region $\omega_M(t)$ may

be unambiguously defined and there LR occurs efficiently. A substantial fraction of particles outside the homogeneous ion core does not undergo this LR.

Moreover, for a short pulse <50 fs [34] or at early times of a long pulse, the expansion of the ionic background is insufficient to meet the above conventional LR. In this case nonlinear resonance (NLR) was identified as the leading collisionless mechanism of efficient laser absorption in Refs. [34–38]. NLR occurs when the excitation energy-dependent eigenfrequency of a (laser-driven) electron in the self-consistent, anharmonic cluster potential meets the laser frequency ω .

The conventional dual-pulse LR in the expanding stage of a cluster is less efficient than a LR during the early cycles of a single, short, laser pulse when the cluster is still compact [39]. By particle-in-cell (PIC) simulations of xenon clusters it was envisaged that early LR requires intense, short pulses of ultraviolet wavelength near 125 nm [39]. However, experiments close to this wavelength are rare, except for a few at free electron lasers [40–42] and x-ray lasers of wavelength below 100 nm [43] and intensities $<10^{15}$ W cm⁻². On the other hand, subcycle (SC) [44,45], single-cycle [46–49], and extreme few-cycle laser pulses with near relativistic peak intensity [50,51] were reported and stimulated research activities for direct acceleration of electrons [52]. These ultrashort broadband pulses may open another promising route toward efficient absorption without significant cluster expansion. The rather broad ω_M (due to charge inhomogeneity) may overlap with some part of the broad frequency spectrum of the near-single-cycle pulse to yield higher absorption via early LR. The decrease of the relative density $\rho/\rho_c(\omega) > 1$, [$\rho_c(\omega) = \omega^2/4\pi$ is the critical density at ω] with respect to the higher ω may drive NLR with a greater efficiency [35,36] together with LR.

In this work, we report on the regime of laser-cluster interaction with pulse durations τ below one optical period $T = \lambda_0/c$ at the central wavelength $\lambda_0 = 800$ nm. In this case the ponderomotive energy $U_p = E_0^2/4\omega^2$ (i.e., the average kinetic energy of a free electron in a monochromatic laser field of frequency ω and field strength E_0) cannot be uniquely defined. Our goal is to investigate the nature of energy absorption with extremely short pulses.

Since the cluster radius $R_0 \ll \lambda$, the dipole approximation is applicable, and the effect of $\mathbf{v} \times \mathbf{B}$ is negligible as long as the laser intensity $< 10^{18} \text{ W cm}^{-2}$, which is the case in this work. However, previously used conventional \sin^2 pulses [35–37,53] or Gaussian pulses [34,54–57] for the laser electric field $E(t)$ cannot be used in the near-single-cycle and subcycle regime since they yield nonzero value of the integral $\int_{t_i}^{t_f} E(t)dt$ over the pulse duration $t_i \rightarrow t_f$, which results in an unphysical energy gain even by a free charge [58]. In Sec. II we introduce two pulse models that are valid in the SC regime. We study energy absorption by a rigid sphere model (RSM) of a cluster [37] and by more realistic three-dimensional PIC simulations [35,36] for deuterium clusters in Secs. III and IV and argon clusters in Sec. V. In Sec. VI we conclude and summarize the results.

II. LIGHT PULSE IN THE SUBCYCLE REGIME

First we consider a widely used Gaussian pulse $E(t) = \text{Re}[E_0 \exp(-t^2/2\delta^2) \exp(i\omega t + i\phi_0)]$. Following Ref. [58] the corresponding electric field, valid in the SC regime, can be found as

$$E(t') = \text{Re} \left[-iE_0 \frac{(1 + it'/\omega\delta^2)^2 + 1/(\omega\delta)^2}{1 + 1/(\omega\delta)^2} \frac{p(t')}{p(0)} \right] \quad (1)$$

where $p(t) = p_0 \exp(-t^2/2\delta^2) \exp(i\omega t + i\phi_0)$, $t' = t - t_0$, t_0 is the time when $E(t') = E_0$, and δ is related to the FWHM $\tau = 2\delta\sqrt{2 \ln 2}$. In Ref. [58] it is shown that $I(t) = \int_{-\infty}^{\infty} E(t'')dt''$ does not vanish for the conventional pulse when the pulse duration $\tau < 2T$. For the corrected pulse (1) $I(t) = 0$, irrespective of τ . When $\tau \gg 2T$, the integral $I(t)$ of the corrected pulse and the conventional pulse both vanish, which had allowed various researchers to use conventional Gaussian pulses [34,54–56] for studying laser-cluster interaction in the long-pulse regime.

We consider another widely used conventional model of an n -cycle laser pulse, the \sin^2 pulse $E(t) = E_0 \sin^2(\omega t/2n) \cos(\omega t)$ for $0 < t < nT$ [35–37,53], which in some cases also yields $\int_0^{nT} E(t)dt \neq 0$. For example $n = 1$ gives $\int_0^{nT} E(t)dt = -T/4$. To overcome this unphysical feature we use the vector potential $A(t) = (E_0/\omega) \sin^2(\omega t/2n) \cos(\omega t)$ for $0 < t < nT$ and compute the electric field $E(t) = -dA/dt$ as

$$E(t) = (E_0/\omega) \begin{cases} \sum_{i=1}^3 c_i \omega_i \sin(\omega_i t) & 0 < t < nT \\ 0 & \text{otherwise} \end{cases} \quad (2)$$

with $c_1 = 1/2$, $c_2 = c_3 = -1/4$, $\omega_1 = \omega$, $\omega_2 = (1 + 1/n)\omega$, $\omega_3 = (1 - 1/n)\omega$. Figures 1(a)–1(c) show the waveform of $E(t)$ of the conventional \sin^2 pulse [light gray (green)] and the corrected pulse [dark gray (red)] (2) for different values of $\tau = 2T, T, 3T/4$. The corresponding integrals $I(t)$ are shown in Figs. 1(d)–1(f) with conventional [light gray (green)] and corrected [dark gray (red)] pulses. For $\tau = 2T$, the integral $I(t)$ of the corrected pulse [in Fig. 1(d)] and the conventional pulse vanishes exactly. As τ approaches T (e.g., for $\tau = T$ [Figs. 1(b) and 1(e)]) $I(t)$ of the conventional \sin^2 pulse strongly deviates from zero [in Fig. 1(e)] at the end of the pulse. This deviation remains [in Fig. 1(f)] for subcycle pulses [in Fig. 1(c)] of $\tau = 3T/4$. In all cases [Figs. 1(d)–1(f)] the

corrected pulse (2) leads to $\int_0^{nT} E(t)dt = 0$ and thus prohibits unphysical energy transfer to the cluster particles.

The spectra for the fields (1) and (2) are broad. For instance, ω_2 in (2) assumes values $2\omega, 3\omega$ for $n = 1, 1/2$ respectively. We shall mostly use (2) unless explicitly mentioned.

III. LASER ABSORPTION IN DEUTERIUM CLUSTERS VERSUS PULSE DURATION

Due to the delicate dependency of laser energy absorption on cluster size [18,24,55,59], laser wavelength [39,54,55,59], peak intensity [24,34–36,55,57,59,60], and pulse duration $\tau \gg 2T$ [24,53,55,56,59,61–63], it is difficult to predict which combination of parameters will lead to efficient absorption. Experiments [24] and two-dimensional PIC simulations [56] with rare-gas clusters for a fixed pulse energy and cluster size showed that energy absorption increases initially with increasing τ up to a value between $100T$ – $150T$ (at 800 nm), then reaches a peak value, and decreases for very long picosecond pulses. These results were explained on the basis of the LR. However, we restrict τ below 50 fs where the conventional LR does not occur. Although our results for $\tau > 2T$ agree qualitatively with previous works [24,56], they are entirely different in nature for $\tau < 2T$. Recent experiments [62,63] with sub-10 fs (FWHM) pulses demonstrated already a different nature of ion emission from clusters.

In this section we consider the interaction of a deuterium cluster of radius $R_0 = 2.2 \text{ nm}$ (number of atoms $N = 2176$) and charge density $\rho = 27.86\rho_c(\omega)$ (i.e., $\omega_M \approx 3\omega$) with laser pulses in the multicycle down to the subcycle regime with the peak intensity fixed. The radius R_0 of a cluster is estimated from the number of atoms N through $R_0 = r_0 N^{1/3}$, with r_0 the Wigner-Seitz radius that depends on the cluster type (e.g., for deuterium and argon cluster $r_0 = 0.17 \text{ nm}$ and 0.24 nm , respectively).

A. Absorption study with a rigid sphere model

First we study energy absorption with a simple rigid sphere model (RSM) of a cluster [35–37]. In the RSM the cluster is regarded as a spherical pre-ionized plasma of homogeneous charge density. The center of the negatively charged electron sphere initially coincides with the center of the positively charged ion sphere. During the short duration of the laser pulse the massive ion-sphere is considered immobile. Although the RSM is a simple model it qualitatively reproduced many results of realistic PIC simulations [35,36] in the past.

In a linearly (along x) polarized laser field $E(t)$ the equation of motion of the electron sphere can be written as

$$\ddot{\mathbf{x}} + g(r)\mathbf{x}/r = -\hat{\mathbf{x}}E(t), \quad (3)$$

where $r = |\mathbf{x}|$ is the displacement of the electron sphere, and $g(r)$ is the electrostatic restoring force which reads

$$g(r) = \omega_M^2 \begin{cases} r + \alpha r^2 + \beta r^4 & 0 \leq r \leq 2R_0 \\ \gamma/r^2 & r \geq 2R_0 \end{cases}. \quad (4)$$

Here $\alpha = -9/16R_0$, $\beta = 1/32R_0^3$, and $\gamma = 1$. As the electron sphere moves away from the center $r = 0$ of the ion sphere, $g(r)$ changes from harmonic to anharmonic, and finally Coulombic behavior for $r \geq 2R_0$ [35–37]. The pulse profile

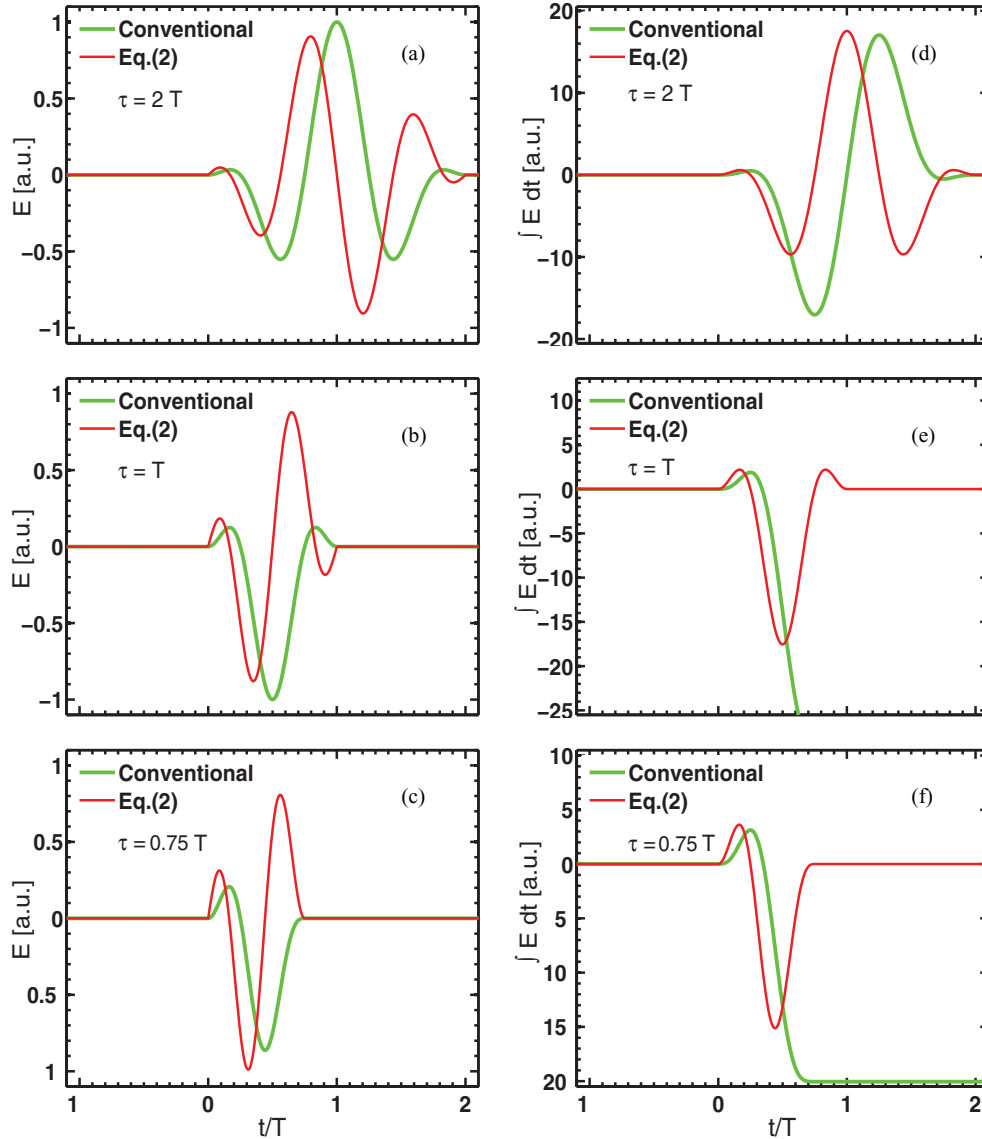


FIG. 1. (Color online) Temporal variation of a conventional \sin^2 pulse $E(t) = E_0 \sin^2(\omega t/2n) \cos(\omega t)$ [light gray (green) in (a), (b), and (c)] and the corresponding corrected pulse (2) [dark gray (red) in (a), (b), and (c)] for various pulse lengths $\tau = 2T, T, 3T/4$. The integral $I(t) = \int_{t_i}^t E(t'') dt''$ is shown in (d), (e), and (f). The central wavelength is $\lambda_0 = 800$ nm and $E_0 = 1$ a.u.. The integral $I(t)$ of the conventional pulse [(light gray (green))] does not always vanish for $\tau \leq T$.

$E(t)$ can be chosen according (1) or (2). The energy E_a absorbed by the cluster (of mass m_s and total charge of the electron sphere q_s) is calculated as $E_a = E_a(\tau) = m_s \dot{x}^2/2 + q_s \int g(r) dr$.

Before we study the absorption by the above anharmonic oscillator it is worth examining the corresponding harmonic oscillator (HO) by setting $\alpha = \beta = \gamma = 0$. For analytical tractability we use (2) for $E(t)$ and find

$$x = \sum_{k=1}^3 a_k [\sin(\omega_k t) - \omega_k \sin(\omega_M t)/\omega_M] / (\omega_M^2 - \omega_k^2), \quad (5)$$

with $x(0) = \dot{x}(0) = 0$ and $a_k = -E_0 c_k \omega_k / \omega$. The absorbed energy in this case is simply $E_a = m_s v^2/2 + q_s \omega_M^2 x^2/2$ and plotted (normalized to NU_p) vs τ/T in Fig. 2, showing that E_a/NU_p increases [thin solid black (blue)] with decreasing

τ/T from $\tau/T = 2$ (with a faster rise of E_a/NU_p for $\tau/T \lesssim 1$), reaches a peak between $\tau/T \approx 0.3-0.4$, and then drops with further decrease of τ/T . The energy absorption by the HO in Fig. 2 can be illustrated by the dynamics of the electron sphere in the (x, v) -phase space (x and v are normalized by R_0 and the quiver velocity $v_0 = E_0/\omega$, respectively) in Fig. 3 for different values of $n = \tau/T = 4, 2, 1, 0.5$. As n increases, the electron sphere undergoes more and more oscillations and tends to come back to its initial point in phase space. For $n \rightarrow \infty$ the electron sphere is driven with a single frequency ω far below the linear resonance $\omega_M \approx 3\omega$. It returns to its initial point after the pulse is over, and no net energy absorption takes place [37]. The situation changes as τ/T shortens. Already at $\tau/T = 4$ [in Fig. 3(a)] one sees that the phase-space trajectory is not closed. The distance of the initial point to the final point also increases with decreasing

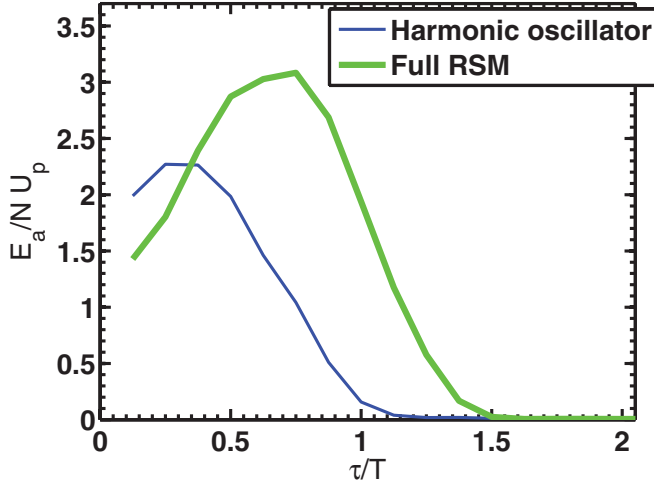


FIG. 2. (Color online) Normalized absorbed energy E_a/NU_p vs pulse duration τ/T in the RSM [thick solid gray (green)] and harmonic oscillator [thin solid black (blue), with $\alpha = \beta = \gamma = 0$ in Eq. (4)] using (2). The Deuterium cluster of radius $R_0 = 2.2$ nm ($N = 2176$), charge density $\rho = 27.86\rho_c$ is irradiated by laser pulses of central wavelength $\lambda_0 = 800$ nm and peak intensity 5×10^{15} W cm $^{-2}$.

$\tau/T = 4, 2, 1, 0.5$, leading to the increased energy absorption in Fig. 2 for the HO. As τ/T is decreased from $1 \rightarrow 0.5$ the frequency component ω_2 changes $2\omega \rightarrow 3\omega$, and the HO passes from near resonance to resonance where both excursion x and velocity v are substantially increased [Figs. 3(c) and 3(d)]. For the lowest value $\tau/T = 1/8$ considered in this work both frequency components ω_2, ω_3 exceed ω_M , the plasma becomes underdense with respect to them, and the absorption drops. The above results clearly show that, contrary to the known long-pulse scenario, a harmonic oscillator driven by ultrashort pulses may gain energy by retaining a phase different from its initial value.

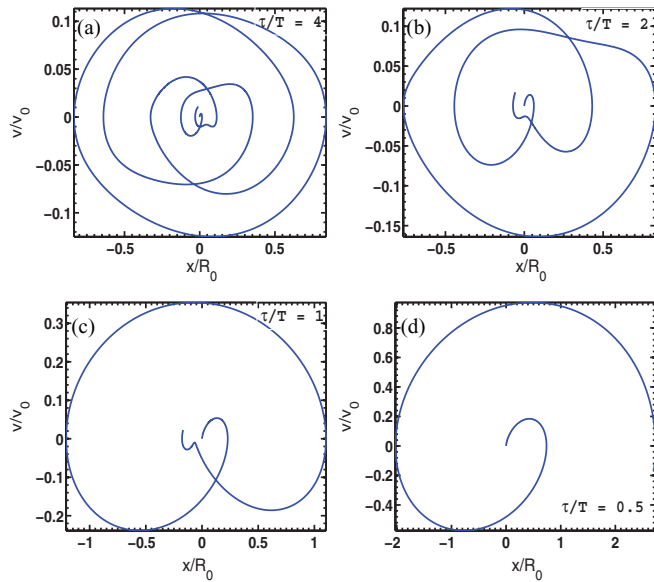


FIG. 3. (Color online) Phase space (x, v) diagram for the harmonic oscillator at various $\tau/T = 4, 2, 1, 0.5$, corresponding to the parameters of Fig. 2.

In the above harmonic oscillator approximation the electron sphere moves in an infinitely deep parabolic potential. After the pulse the whole electron cloud will continue to oscillate with ω_M . In reality, however, electrons may leave the cluster (outer ionization), sensing the Coulomb tail of the potential due to the net charge left behind. The RSM (4) has this property, and the electron sphere may undergo LR and/or NLR, depending upon the frequencies in the driver. As soon as the electron sphere comes close to the resonance (either LR or NLR) the final (x, v) differs from its initial value. Solving the RSM (3)–(4) numerically we compare E_a/NU_p vs τ/T for the full RSM with the HO in Fig. 2. Both RSM and HO show that E_a/NU_p increases as τ/T decreases, reaches a maximum below $\tau/T = 1$ and then drops for very low τ/T . In case of the RSM the phase-space trajectory starts becoming more chaotic due to the nonlinearity in $g(r)$, leading to a faster rise in E_a/NU_p already at a bigger τ/T (~ 1.5) and a shift of the peak position towards $\tau/T = 1$. For the HO, E_a/NU_p vs τ/T and the peak position are independent of the peak intensity $I_0 = E_0^2$. This is not the case for the RSM due to the intensity-dependent eigenperiod determining the NLR.

B. Particle-in-cell results

In this section we study the energy absorption with more realistic three-dimensional PIC simulations [18,39]. In our PIC simulation, initially the laser field $E(t)$ ionizes all neutral atoms X to X^+ via over-the-barrier ionization [64] after reaching a critical value $E(t) \geq I_p(Z)^2/4Z$ [where $I_p(Z)$ is the ionization potential for charge state Z]. Subsequent displacement of electrons by the laser field creates a space charge field E_{sc} , and further ionization is governed by the condition $|E(t)\hat{x} + E_{sc}(t, \mathbf{R}_i)| \geq I_p(Z)^2/4Z$, for an ion at position \mathbf{R}_i . A PIC electron has the same charge to mass ratio as a real electron. The equation of motion of the i th PIC electron is $\ddot{\mathbf{r}}_i = -\hat{x}E(t) - E_{sc}(t, \mathbf{r}_i)$ whereas the j th ion of mass M_j and charge Z_j obeys $M_j \ddot{\mathbf{R}}_j = Z_j[\hat{x}E(t) + E_{sc}(t, \mathbf{R}_j)]$. The space charge field E_{sc} is obtained by solving Poisson's equation on the numerical grid. The field is then interpolated to the particle positions, and the equations of motion for the particles are solved using the Runge-Kutta method. The total absorbed energy $E_a(t)$ is obtained by summing over the kinetic energies of all particles (electrons and ions) plus the electrostatic field energy. The numerical parameters in our PIC simulations (spatial and temporal resolution, grid size, number of PIC particles, etc.) were carefully chosen such that artificial numerical heating was negligible.

1. Energy absorption and outer ionization

The same deuterium cluster of radius $R_0 = 2.2$ nm is irradiated with various peak intensities and pulse durations with $E(t)$ according to (2). Figure 4 shows the scaled energy $E_a(\tau)/NU_p$ vs τ/T for intensities 5×10^{15} W cm $^{-2}$ [dark gray (red)] and 10^{16} W cm $^{-2}$ [light gray (green)]. The vertical dashed line at $\tau/T = 1$ indicates the onset of the subcycle regime. A clearly distinct behavior of $E_a(\tau)/NU_p$ is observed for $\tau/T < 2$ and $\tau/T > 2$. At 5×10^{15} W cm $^{-2}$ the absorbed energy increases for $2 < \tau/T < 12$ before it saturates. At the higher intensity 10^{16} W cm $^{-2}$ a similar variation is observed. The qualitative nature of energy absorption beyond $\tau/T > 2$

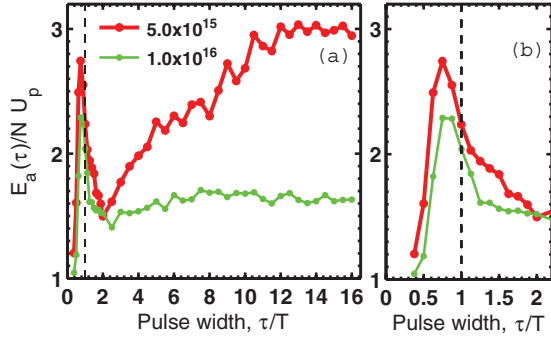


FIG. 4. (Color online) PIC results for the absorbed energy E_a/NU_p per cluster ion N in units of U_p vs pulse duration τ/T for peak intensities $5.0 \times 10^{15} \text{ W cm}^{-2}$ [dark gray (red)] and $10^{16} \text{ W cm}^{-2}$ [light gray (green)]. (b) is the expanded view of (a) for $\tau/T < 2$. Other laser and cluster parameters are as in Fig. 2.

confirms the results in Ref. [56] for deuterium clusters in long pulses. However, $E_a(\tau)/NU_p$ also increases as τ/T drops below 2, with a maximum at ≈ 0.8 . Decreasing τ/T further below 0.8, $E_a(\tau)/NU_p$ decreases again (similar to the RSM results in Fig. 2). The peak values of E_a/NU_p in this subcycle regime are similar or even higher than for longer pulses of the same intensity.

Without the efficient outer ionization the increased absorption in the subcycle regime is certainly not possible. Figure 5 shows the degree of outer ionization n_{out}/N (n_{out} being the number of electrons that already left the cluster) vs τ/T , also demonstrating a clearly distinct behavior below $\tau/T \approx 2$ and above. For long pulses outer ionization gradually increases and saturates ($n_{\text{out}}/N \approx 1$ means 100% outer ionization, i.e., complete removal of all electrons from the cluster). Below $\tau/T = 2$, outer ionization also increases (with decreasing τ/T), reaching the peak value $n_{\text{out}}/N \approx 1$ at $\tau/T = 0.8$ before it drops again. Hence, our results clearly show that outer ionization and energy absorption go together.

2. Explanation for absorption and outer ionization

The absorption mechanism and the peak position at $\tau/T \approx 0.8$ for $E_a(\tau)/NU_p$ of Fig. 4 and n_{out}/N of Fig. 5 can be explained by comparing the different frequency components $\omega_i = \omega_1, \omega_2, \omega_3$ in (2) and the Mie-plasma frequency

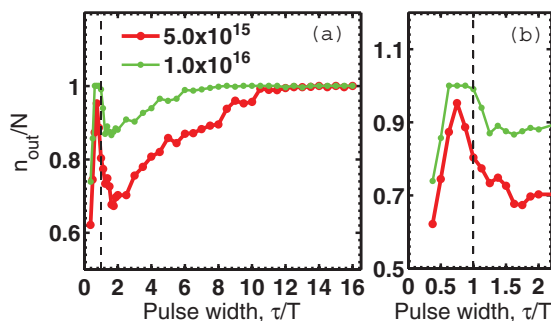


FIG. 5. (Color online) PIC results for outer ionization n_{out}/N vs τ/T for the same peak intensities $5.0 \times 10^{15} \text{ W cm}^{-2}$ [dark gray (red)] and $10^{16} \text{ W cm}^{-2}$ [light gray (green)] as in Fig. 4. (b) is the expanded view of (a) for $\tau/T < 2$.

$\omega_M = \sqrt{4\pi\rho/3} \approx 3\omega$ of the deuterium cluster. We found [35] that for long pulses ($\tau/T = 2-16$, $\omega_M > \omega_i$, i.e., plasma remains overdense) the absorption process is due to NLR. For $\tau/T = 1$, one finds $\omega_i = \omega, 2\omega, 0$. Hence, our interpretation is that the plasma is marginally overdense with respect to $\omega_2 = 2\omega$ and the NLR becomes more efficient due to the decrease of the relative density $\rho/\rho_c(\omega_2)$ with respect to $\omega_2 = 2\omega$. Thus, in passing from $\tau/T = 2$ to $\tau/T = 1$, increased absorption and outer ionization may occur because of the gradual decrease of the ratio $\rho/\rho_c(\omega_2)$ with respect to ω_2 that drives the NLR more efficiently. For $\tau/T = 0.5$, the frequencies are $\omega_i = \omega, 3\omega, \omega$. The laser pulse becomes $E(t) = E_0[\sin(\omega t)/4 - 3\sin(3\omega t)/4]$. In this case LR (for the 3ω component) and NLR (for the ω component) may occur simultaneously but the opposite polarity of the two components reduce each others contribution, resulting in absorption and outer ionization below the respective peak values. Moreover, for such a short pulse the temporal width of the LR at early times is too small to have a significant effect. Just meeting the resonance condition is not enough. Both a high driver strength and enough time close to the resonance are important for efficient absorption. With a much shorter $\tau/T = 0.25$ (where $\omega_i = \omega, 5\omega, 3\omega$) the plasma becomes underdense with respect to $\omega_2 = 5\omega$, for which neither NLR nor LR works. The LR at $\omega_3 = 3\omega$ (and the NLR at $\omega_1 = \omega$) is less efficient than the LR at $\omega_2 = 3\omega$ with a higher $\tau/T = 0.5$. From the above discussion, the peak in the absorbed energy and outer ionization for a certain τ/T between 0.25 and 1 (in our case $\tau/T \approx 0.8$) is understandable: the plasma changes from marginally overdense via critically dense to underdense with respect to a frequency component of the driver. Interestingly, the peak position and peak value of E_a/NU_p nearly matches with the RSM in Fig. 2 for the same intensity $5 \times 10^{15} \text{ W cm}^{-2}$.

3. Absorption and outer ionization with Gaussian pulse

We performed analogous PIC simulations for the Gaussian pulse (1). E_a/NU_p and n_{out}/N vs τ/T are plotted in Fig. 6, showing a qualitatively similar behavior as in Figs. 4 and 5,

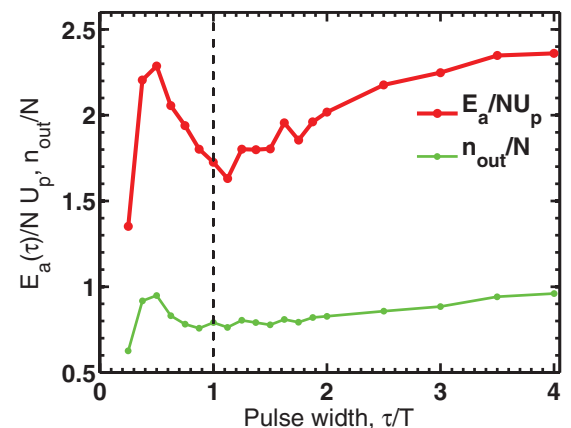


FIG. 6. (Color online) PIC results for absorbed energy E_a/NU_p [dark gray (red)] and outer ionization n_{out}/N [light gray (green)] vs τ/T for a pulse (1) at peak intensity $5.0 \times 10^{15} \text{ W cm}^{-2}$. Other parameters are as in Fig. 2.

respectively, except that the subcycle maximum and the turning point separating the subcycle from the multicycle behavior are shifted to a lower value of τ/T . For the Gaussian pulse shape, the laser electric field $E(t)$ cannot be separated into discrete frequencies, so that a part-by-part analysis as above is not possible.

C. Efficiency of laser absorption

From the results shown so far (both RSM and PIC) it is clear that laser absorption is very efficient for pulse durations $\tau/T < 2$. We may define the efficiency $\eta = (E_a/E_d)/\max(E_a/E_d)$ of laser absorption, where $E_d \propto \lambda_0^2 \int_{t_i}^{t_f} E(t)^2 dt$ is the energy contained in the laser pulse.

Figure 7 shows η vs τ/T for peak intensities 5.0×10^{15} , 10^{16} , 5.0×10^{16} , 10^{17} W cm $^{-2}$ with RSM [Fig. 7(a)] and PIC [Fig. 7(b)] and a \sin^2 pulse (2). For a given peak intensity η increases as τ/T decreases. η becomes unity at a $\tau/T < 1$ (near 0.8), and drops toward zero for $\tau/T \ll 1$. For a very low $\tau/T \rightarrow 0$, the plasma is underdense with respect to the frequencies of the driver and $E_d \rightarrow 0$, thus giving $\eta \rightarrow 0$. The oscillatory behavior of η vs τ/T [in Fig. 7(a)] is due to the different phases the electron sphere in the RSM has

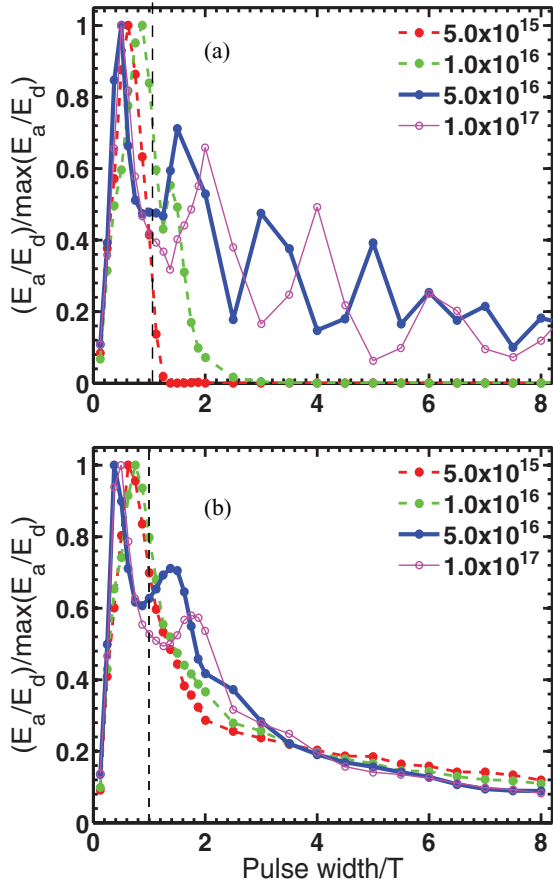


FIG. 7. (Color online) Energy absorption efficiency $\eta = (E_a/E_d)/\max(E_a/E_d)$ vs pulse duration τ/T at various peak intensities 5.0×10^{15} [dashed-black (red)], 10^{16} [dashed-gray (green)], 5.0×10^{16} [thick dark gray (blue)], 10^{17} W cm $^{-2}$ [thin gray (pink)] with (a) RSM (top figure), and (b) PIC (bottom figure) using $E(t)$ according to (2). Other parameters as in Fig. 2.

in (x, v) -space after the pulse. However, the average η in the RSM [Fig. 7(a)] for intensities $\geq 5 \times 10^{16}$ W cm $^{-2}$ matches with the corresponding PIC results in Fig. 7(b). For relatively low intensities $< 5 \times 10^{16}$ W cm $^{-2}$ (but above the intensity required for ionization) the absorption efficiency in the RSM is very small for $\tau/T > 2$, and abruptly jumps up as τ/T is decreased below 2. This sudden jump is due to the artifact of the RSM that the whole electron cloud behaves as one huge pseudoparticle. The outer ionization of the whole cloud represents the complete removal of all electrons from the cluster at the same time. In PIC simulations, the electrons are gradually emitted at different times. As a result, such a sudden jump in E_a , and oscillations in η [as seen in Fig. 7(b) for the RSM] are averaged out in PIC. Although the RSM is a very simplified model of a cluster it overall compares well with the PIC results.

IV. DEUTERIUM CLUSTER AT A FIXED ENERGY LASER PULSE OF VARIABLE PULSE DURATION

The laser pulses considered above were of fixed intensity so that the pulse energy E_d increases with increasing τ . In experiments, however, one may wish to keep the laser energy fixed and change τ (see Ref. [24]). For completeness, we have carried out PIC simulations with $E(t)$ according to (2) for the same deuterium cluster as in the previous section but keeping the laser energy (per cm 2) $I_0 \times n_0 T$ fixed. The pulse duration changes, $\tau = nT$, so that $I_{\text{peak}} = I_0 \times n_0/n$. For convenience we fix $n_0 = 1$, $I_0 = 10^{16}$ W cm $^{-2}$. For this set of parameters $I_{\text{peak}} = 10^{15}$, 10^{16} , 10^{17} W cm $^{-2}$ for $n = \tau/T = 10$, 1, 0.1, respectively.

Absorbed energy $E_a/\max(E_a)$ and outer ionization n_{out}/N as a function of the pulse duration τ/T are plotted in Fig. 8. A slow variation of $E_a/\max(E_a)$ and n_{out}/N is seen when τ/T is decreased from 10 to 2. Decreasing τ/T further, the slopes of $E_a/\max(E_a)$ and n_{out}/N increase drastically and reach a peak near $\tau/T \approx 0.8$, similar to the results in Figs. 4 and 5. Since the pulse energy is kept fixed and thus the intensity is high

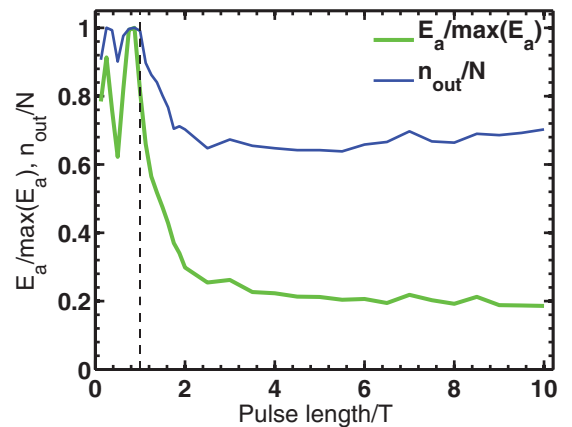


FIG. 8. (Color online) PIC results for normalized energy absorption $E_a/\max(E_a)$ [light gray (green)], outer ionization n_{out}/N [dark gray (blue)] vs τ/T for the same Deuterium cluster as in Fig. 2 with pulse (2). The pulse energy was fixed (see text). Other parameters as in Fig. 2.

for ultrashort pulses (e.g., $10^{17} \text{ W cm}^{-2}$ for $\tau/T \approx 0.1$), the absorbed energy and outer ionization do not drop as $\tau \rightarrow 0$.

The second peak at $\tau \simeq T/4$ and the minimum in between close to $\tau = T/2$ in absorbed energy and outer ionization is probably due the amplification/reduction of the field amplitude due to different frequencies in (2) when $\tau < T$. To simplify the discussion we consider the first peak being at $n \simeq 1$ (instead of $n = 0.8$). We rewrite (2) for $n = 1, 1/2, 1/4$ as $E(t) = E_0[\sin(\omega t)/2 - \sin(2\omega t)/2]$, $E(t) = \sqrt{2}E_0[\sin(\omega t)/4 - 3\sin(3\omega t)/4]$, and $E(t) = 2E_0[\sin(\omega t)/2 - 3\sin(3\omega t)/4 - 5\sin(5\omega t)/4]$, respectively. The overall prefactors are due to the $\sqrt{1/n}$ dependence in case of constant fluence. One can see that the amplitudes of the high-frequency components increase with shortening of the pulse. Some of these high-frequency components may meet LR with significant driving strength. The strength of the ω component first drops from $E_0/2$ to $E_0/(2\sqrt{2})$ and then increases to E_0 for $n = 1, 1/2, 1/4$, respectively. Also the amplitude of the 3ω component (note that this is close to the Mie-resonance frequency ω_M for the deuterium cluster) increases from $3E_0/(2\sqrt{2})$ to $3E_0/2$ when $n = 1/2$ and $1/4$, respectively. This indicates that the resonance at $n = 1/4$ will lead to a higher absorbed energy than the resonance at $n = 1/2$. The factor by which this enhancement occurs may be estimated by the ratio of the square of the amplitudes of the field at $n = 1/4$ and $n = 1/2$, respectively, which is 2. However, due to other terms in the equation for the field this enhancement is actually reduced, and we may assume it being a factor closer to 1.5. Now we may multiply the value of the normalized absorbed energy 0.6 at $n = 1/2$ (in Fig. 8) with the approximate enhancement factor 1.5, which justifies its value close to 0.9 at $n = 1/4$. We see that by such a reasoning we may qualitatively explain why the absorbed energy shows a double-peak structure with peaks at $n = 1/4$ and 1, and a minimum around $n = 1/2$. However, our observation of the double-peaked structure and its analysis are based on a \sin^2 -shaped vector potential (having three discrete frequencies in the spectrum [see Eq. (2)] and a constant pulse energy even down to the extreme subcycle regime, which is experimentally difficult to achieve.

V. ARGON CLUSTER AT DIFFERENT PULSE DURATIONS: ABSORPTION, CHARGING, AND OUTER IONIZATION

We now present PIC results for argon clusters ($R_0 \approx 3.11 \text{ nm}$, $N = 2176$), using again (2) for $E(t)$. For deuterium clusters inner ionization saturates as soon as the laser field liberates the bound electrons. The absence of an additional supply of electrons results in saturation of energy absorption [56] and outer ionization for long pulses. The corresponding peak values in the absorbed energy and outer ionization at $\tau \approx 0.8T$ may also be attributed to this effect of saturation of inner ionization. However, for (multi-electron atom) Ar clusters inner ionization may continue through the ionization ignition [27–32].

To identify whether the charged cluster passes LR it is important to know $\omega_M(t)$. For this one may attempt to use the relation $\omega_M(t) = \sqrt{NZ_{av}/R^3(t)}$, where $R(t)$ is the radius of

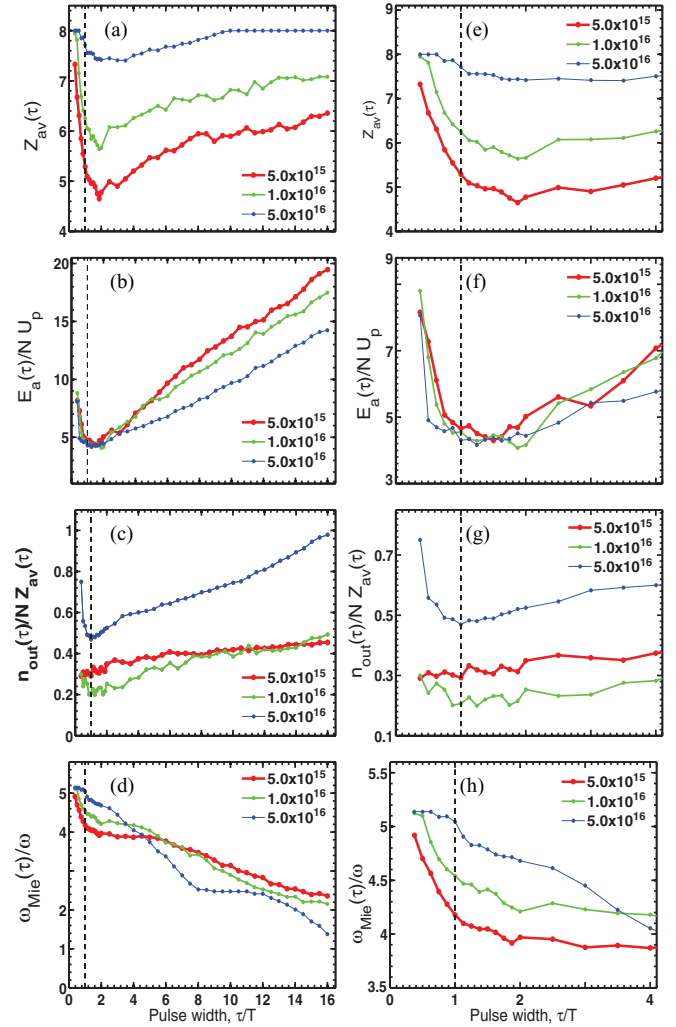


FIG. 9. (Color online) PIC results for Argon clusters ($R_0 = 3.11 \text{ nm}$, $N = 2176$) showing (a) average charge per cluster ion Z_{av} , (b) absorbed energy E_a/NU_p , (c) outer ionization n_{out}/NZ_{av} and (d) the normalized Mie-plasma frequency ω_M/ω vs pulse duration τ/T for peak intensities $5.0 \times 10^{15} \text{ W cm}^{-2}$ [thick gray (red)], $10^{16} \text{ W cm}^{-2}$ [light gray (green)], and $5 \times 10^{16} \text{ W cm}^{-2}$ [thin black (blue)]. The plots (e)–(h) are the expanded view of (a)–(d) respectively. Laser wavelength $\lambda_0 = 800 \text{ nm}$ and laser profile (2) as in Fig. 4.

the expanding cluster at time t . Due to the faster disintegration of ions near the cluster boundary and the inhomogeneous charge distribution such a $\omega_M(t)$ underestimates the actual ω_M . Instead, the ionic charge distribution within R_0 is found to be almost homogeneous, and we use $\omega_M(t) = \sqrt{Q_b(t)/R_0^3}$ [18,39] with $Q_b(t)$ as the total charge within R_0 at a time t .

Figures 9(a) and 9(e) show the average charge Z_{av} per cluster ion, [Figs. 9(b) and 9(f)] the absorbed energy E_a/NU_p , [Figs. 9(c) and 9(g)] the outer ionization n_{out}/NZ_{av} , and [Figs. 9(d) and 9(h)] the normalized Mie-plasma frequency ω_M/ω vs the pulse duration τ/T for peak intensities $5.0 \times 10^{15} \text{ W cm}^{-2}$, $10^{16} \text{ W cm}^{-2}$, and $5.0 \times 10^{16} \text{ W cm}^{-2}$. Figures 9(e)–9(h) are the expanded views of Figs. 9(a)–9(d), respectively. With higher peak intensity, Z_{av}, n_{out}, E_a increase

for all pulse durations, which is expected. Above $\tau/T = 2$, the values of Z_{av} , E_a/NU_p , and n_{out}/NZ_{av} increase with increasing τ/T , while ω_M/ω decreases due to Coulomb expansion. This variation of the absorbed energy in long pulses agrees qualitatively with earlier works [24,56]. Z_{av} saturates at $Z_{av} = 8$ and $\tau/T > 10$ for the highest pulse intensity $5 \times 10^{16} \text{ W cm}^{-2}$ plotted due to the removal of all electrons of inner to (including) the $3s$ shell of all atoms (saturation of inner ionization). However, E_a/NU_p continues to increase due to the continuous increase of n_{out}/NZ_{av} up to unity at $\tau/T = 16$. Note that ω_M/ω does not drop to unity so that conventional LR is not met [35–37].

The saturation of E_a/NU_p and n_{out}/NZ_{av} at longer τ/T , as seen for deuterium clusters [in Figs. 4(a) and 5(a) with $Z_{av} = 1$] is absent here due to additional supply of electrons NZ_{av} through ongoing inner ionization. At a given pulse duration and intensity, n_{out}/NZ_{av} [in Fig. 9(c)] is smaller than for deuterium. By multiplication with the corresponding Z_{av} the number of electrons n_{out} actually expelled from the Ar cluster is found to be higher, which explains higher absolute energy gain in Fig. 9(b) compared to the deuterium case at the same pulse duration and intensity. At $\tau/T = 12$, for instance, for the intensity $10^{16} \text{ W cm}^{-2}$ we find $n_{out}/NZ_{av} \approx 0.4$ and $Z_{av} \approx 7$, giving $n_{out} \approx 2.8N$, which is significantly higher than for the deuterium case where $n_{out} \approx N$. The absorbed energy E_a/NU_p is also larger because of higher n_{out} , higher electrostatic field due to $Z_{av} > 1$, and higher kinetic energy of Ar ions.

The dependence of E_a/NU_p and n_{out}/NZ_{av} on τ/T for $\tau/T \leq 2$ is similar to the case of the deuterium cluster in Figs. 4 and 5 but the peak disappears because of the continuous increase of Z_{av} with additional inner ionization as the pulse is made shorter. With increasing peak intensity Z_{av} starts at a higher value at $\tau/T = 2$, saturates soon at $Z_{av} = 8$, corresponding to the removal of all electrons from the M shell of all Ar atoms. Unless the laser intensity is increased beyond a few times $10^{18} \text{ W cm}^{-2}$ or the cluster size is increased, a charge state $Z_{av} \geq 9$ by ionizing the next shell is difficult to obtain. The relative increase of Z_{av} at a lower intensity is higher than that at a higher intensity (Z_{av} increases from 4.6 to 7.4 for $5 \times 10^{15} \text{ W cm}^{-2}$ while at a 10 times higher intensity $5 \times 10^{16} \text{ W cm}^{-2}$, Z_{av} increases only from 7.5 to 8). This

suggests that the biggest fraction of the absorbed laser energy at relatively low intensity is spent to create highly charged ions that counteract outer ionization. As inner ionization saturates earlier at higher intensity, the remaining pulse energy goes into a quicker increase of E_a/NU_p and n_{out}/NZ_{av} .

Instead of nearly constant $\omega_M(t)$ for $\tau/T < 2$ in the deuterium case, $\omega_M(t)$ for the argon cluster changes due to $Z_{av}(t)$. During the charging of the argon cluster from $Z_{av} = 1, 2, 3, \dots, 8$ in steps, $\omega_M(t)$ changes as $\omega_M(t) \approx 1.83\omega, 2.58\omega, 3.16\omega, \dots, 5.16\omega$, respectively. At a given pulse duration $\tau < 2T$, some of those $\omega_M(t)$ either dynamically meet the corresponding ω_i , leading to LR, or remain just above ω_i , leading to possible NLRs, as already described for the deuterium cluster.

VI. CONCLUSION

The regime of laser-cluster interaction at laser-pulse durations τ below the optical period T (at 800 nm) was investigated employing a rigid sphere model (RSM) and self-consistent three-dimensional PIC simulations. In this subcycle regime care has to be exercised as far as the laser-pulse modeling is concerned. We showed that for a fixed peak intensity of the laser-pulse energy absorption and outer ionization as functions of τ increase as $\tau \lesssim 2T$ decreases, despite the decreasing pulse energy. In the case of deuterium clusters they reach a peak value near $\tau \approx 0.8T$ due to the saturation of inner ionization. Keeping the pulse energy constant, absorption (and outer ionization) also increase with decreasing τ . This, at first sight counterintuitive, behavior was analyzed using harmonic (HO) and anharmonic (RSM) oscillator models. The peak in the absorbed energy at $\tau/T \approx 0.8$ for deuterium clusters disappeared in the PIC results for argon clusters because of ongoing inner ionization. The enhanced absorption, outer ionization and higher charge states of Argon clusters for $\tau/T < 2$ was interpreted in terms of linear and nonlinear resonances.

ACKNOWLEDGMENTS

D.B. is supported by the Deutsche Forschungsgemeinschaft (SFB 652). M.K. thanks S. Sengupta for fruitful discussions.

-
- [1] T. Ditmire, R. A. Smith, J. W. G. Tisch, and M. H. R. Hutchinson, *Phys. Rev. Lett.* **78**, 3121 (1997).
 - [2] T. Ditmire, J. W. G. Tisch, E. Springate, M. B. Mason, N. Hay, J. Marangos, and M. H. R. Hutchinson, *Nature (London)* **386**, 54 (1997).
 - [3] T. Ditmire, J. W. G. Tisch, E. Springate, M. B. Mason, N. Hay, J. P. Marangos, and M. H. R. Hutchinson, *Phys. Rev. Lett.* **78**, 2732 (1997).
 - [4] V. Kumarappan, M. Krishnamurthy, and D. Mathur, *Phys. Rev. Lett.* **87**, 085005 (2001).
 - [5] M. Krishnamurthy, D. Mathur, and V. Kumarappan, *Phys. Rev. A* **69**, 033202 (2004).
 - [6] M. Lezius, S. Dobosz, D. Normand, and M. Schmidt, *Phys. Rev. Lett.* **80**, 261 (1998).
 - [7] V. Kumarappan, M. Krishnamurthy, and D. Mathur, *Phys. Rev. A* **66**, 033203 (2002).
 - [8] Y. Fukuda, K. Yamakawa, Y. Akahane, M. Aoyama, N. Inoue, H. Ueda, and Y. Kishimoto, *Phys. Rev. A* **67**, 061201 (2003).
 - [9] E. Springate, N. Hay, J. W. G. Tisch, M. B. Mason, T. Ditmire, M. H. R. Hutchinson, and J. P. Marangos, *Phys. Rev. A* **61**, 063201 (2000).
 - [10] E. Springate, S. A. Aseyev, S. Zamith, and M. J. J. Vrakking, *Phys. Rev. A* **68**, 053201 (2003).
 - [11] Y. L. Shao, T. Ditmire, J. W. G. Tisch, E. Springate, J. P. Marangos, and M. H. R. Hutchinson, *Phys. Rev. Lett.* **77**, 3343 (1996).
 - [12] V. Kumarappan, M. Krishnamurthy, and D. Mathur, *Phys. Rev. A* **67**, 043204 (2003).

- [13] L. M. Chen, J. J. Park, K. H. Hong, I. W. Choi, J. L. Kim, J. Zhang, and C. H. Nam, *Phys. Plasmas* **9**, 3595 (2002).
- [14] J. W. G. Tisch, T. Ditmire, D. J. Fraser, N. Hay, M. B. Mason, E. Springate, J. P. Marangos, and M. H. R. Hutchinson, *J. Phys. B* **30**, 709 (1997).
- [15] T. D. Donnelly, T. Ditmire, K. Neuman, M. D. Perry, and R. W. Falcone, *Phys. Rev. Lett.* **76**, 2472 (1996).
- [16] C. Vozzi, M. Nisoli, J-P. Caumes, G. Sansone, S. Stagira, S. De Silvestri, M. Vecchiocattivi, D. Bassi, M. Pascolini, L. Poletto, P. Villoresi, and G. Tondello, *Appl. Phys. Lett.* **86**, 111121 (2005).
- [17] B. Shim, G. Hays, R. Zgadzaj, T. Ditmire, and M. C. Downer, *Phys. Rev. Lett.* **98**, 123902 (2007).
- [18] M. Kundu, S. V. Popruzhenko, and D. Bauer, *Phys. Rev. A* **76**, 033201 (2007); S. V. Popruzhenko, M. Kundu, D. F. Zaretsky, and D. Bauer, *ibid.* **77**, 063201 (2008).
- [19] J. Jha, D. Mathur, and M. Krishnamurthy, *J. Phys. B* **38**, L291 (2005).
- [20] J. Jha, D. Mathur, and M. Krishnamurthy, *Appl. Phys. Lett.* **88**, 041107 (2006).
- [21] V. Kumarappan, M. Krishnamurthy, D. Mathur, and L. C. Tribedi, *Phys. Rev. A* **63**, 023203 (2001).
- [22] L. M. Chen, F. Liu, W. M. Wang, M. Kando, J. Y. Mao, L. Zhang, J. L. Ma, Y. T. Li, S. V. Bulanov, T. Tajima, Y. Kato, Z. M. Sheng, Z. Y. Wei, and J. Zhang, *Phys. Rev. Lett.* **104**, 215004 (2010).
- [23] J. Zweiback, R. A. Smith, T. E. Cowan, G. Hays, K. B. Wharton, V. P. Yanovsky, and T. Ditmire, *Phys. Rev. Lett.* **84**, 2634 (2000).
- [24] J. Zweiback, T. Ditmire, and M. D. Perry, *Phys. Rev. A* **59**, 3166 (1999).
- [25] U. Saalman and J. M. Rost, *J. Phys. B* **39**, R39 (2006).
- [26] Th. Fennel, K.-H. Meiwes-Broer, J. Tiggesbäumker, P.-G. Reinhard, P. M. Dinh, and E. Suraud, *Rev. Mod. Phys.* **82**, 1793 (2010).
- [27] C. Rose-Petruck, K. J. Schafer, K. R. Wilson, and C. P. J. Barty, *Phys. Rev. A* **55**, 1182 (1997).
- [28] D. Bauer and A. Macchi, *Phys. Rev. A* **68**, 033201 (2003).
- [29] K. Ishikawa and T. Blenski, *Phys. Rev. A* **62**, 063204 (2000).
- [30] F. Megi, M. Belkacem, M. A. Bouchene, E. Suraud, and G. Zwicknagel, *J. Phys. B* **36**, 273 (2003).
- [31] C. Jungreuthmayer, M. Geissler, J. Zanghellini, and T. Brabec, *Phys. Rev. Lett.* **92**, 133401 (2004).
- [32] D. Bauer, *J. Phys. B* **37**, 3085 (2004).
- [33] T. Ditmire, T. Donnelly, A. M. Rubenchik, R. W. Falcone, and M. D. Perry, *Phys. Rev. A* **53**, 3379 (1996).
- [34] T. Taguchi, T. M. Antonsen Jr., and H. M. Milchberg, *Phys. Rev. Lett.* **92**, 205003 (2004); T. M. Antonsen Jr., T. Taguchi, A. Gupta, J. Palastro, and H. M. Milchberg, *Phys. Plasmas* **12**, 056703 (2005).
- [35] M. Kundu and D. Bauer, *Phys. Rev. Lett.* **96**, 123401 (2006).
- [36] M. Kundu and D. Bauer, *Phys. Rev. A* **74**, 063202 (2006).
- [37] P. Mulser and M. Kanopathipillai, *Phys. Rev. A* **71**, 063201 (2005); P. Mulser, M. Kanopathipillai, and D. H. H. Hoffman, *Phys. Rev. Lett.* **95**, 103401 (2005).
- [38] I. Kostyukov and J. M. Rax, *Phys. Rev. E* **67**, 066405 (2003).
- [39] M. Kundu and D. Bauer, *Phys. Plasmas* **15**, 033303 (2008).
- [40] H. Wabnitz *et al.*, *Nature (London)* **420**, 482 (2002).
- [41] T. Laarmann, M. Rusek, H. Wabnitz, J. Schulz, A. R. B. de Castro, P. Gürtler, W. Laasch, and T. Möller, *Phys. Rev. Lett.* **95**, 063402 (2005).
- [42] C. Bostedt, H. Thomas, M. Hoener, E. Eremina, T. Fennel, K.-H. Meiwes-Broer, H. Wabnitz, M. Kuhlmann, E. Plönjes, K. Tiedtke, R. Treusch, J. Feldhaus, A. R. B. de Castro, and T. Möller, *Phys. Rev. Lett.* **100**, 133401 (2008).
- [43] S. Namba, N. Hasegawa, M. Nishikino, T. Kawachi, M. Kishimoto, K. Sukegawa, M. Tanaka, Y. Ochi, K. Takiyama, and K. Nagashima, *Phys. Rev. Lett.* **99**, 043004 (2007).
- [44] A. E. Kaplan, S. F. Straub, and P. L. Shkolnikov, *Opt. Lett.* **22**, 405 (1997).
- [45] W. J. Chen *et al.*, *Phys. Rev. Lett.* **100**, 163906 (2008).
- [46] P. B. Corkum and F. Krausz, *Nature Phys.* **3**, 381 (2007).
- [47] T. Brabec and F. Krausz, *Rev. Mod. Phys.* **72**, 545 (2000).
- [48] M. Y. Shverdin, D. R. Walker, D. D. Yavuz, G. Y. Yin, and S. E. Harris, *Phys. Rev. Lett.* **94**, 033904 (2005).
- [49] T. Brabec and F. Krausz, *Phys. Rev. Lett.* **78**, 3282 (1997).
- [50] A. J. Verhoeef, J. Seres, K. Schmid, Y. Nomura, G. Tempea, L. Veisz, and F. Krausz, *Appl. Phys. B* **82**, 513 (2006).
- [51] T. Fuji, N. Ishii, C. Y. Teisset, X. Gu, Th. Metzger, A. Baltuska, N. Forget, D. Kaplan, A. Galvanauskas, and F. Krausz, *Opt. Lett.* **31**, 1103 (2006).
- [52] B. S. Xie, M. P. Liu, N. Y. Wang, and M. Y. Yu, *Appl. Phys. Lett.* **91**, 011118 (2007).
- [53] C. Prigent, C. Deiss, E. Lamour, J. P. Rozet, D. Vernhet, and J. Burgdörfer, *Phys. Rev. A* **78**, 053201 (2008).
- [54] G. M. Petrov and J. Davis, *Phys. Plasmas* **13**, 033106 (2006).
- [55] U. Saalman and J. M. Rost, *Phys. Rev. Lett.* **91**, 223401 (2003).
- [56] A. Gupta, T. M. Antonsen, T. Taguchi, and J. Palastro, *Phys. Rev. E* **74**, 046408 (2006).
- [57] M. Arbeiter and T. Fennel, *Phys. Rev. A* **82**, 013201 (2010).
- [58] Q. Lin, J. Zheng, and W. Becker, *Phys. Rev. Lett.* **97**, 253902 (2006).
- [59] T. Martchenko, Ch. Siedschlag, S. Zamith, H. G. Muller, and M. J. J. Vrakking, *Phys. Rev. A* **72**, 053202 (2005).
- [60] T. Döppner, J. P. Müller, A. Przystawik, S. Gode, J. Tiggesbaumker, K.-H. Meiwes-Broer, C. Varin, L. Ramunno, T. Brabec, and T. Fennel, *Phys. Rev. Lett.* **105**, 053401 (2010).
- [61] K. W. Madison, P. K. Patel, M. Allen, D. Price, R. Fitzpatrick, and T. Ditmire, *Phys. Rev. A* **70**, 053201 (2004).
- [62] E. Skopalová, Y. C. El-Taha, A. Zaïr, M. Hohenberger, E. Springate, J. W. G. Tisch, R. A. Smith, and J. P. Marangos, *Phys. Rev. Lett.* **104**, 203401 (2010).
- [63] D. Mathur, F. A. Rajgara, A. R. Holkundkar, and N. K. Gupta, *Phys. Rev. A* **82**, 025201 (2010).
- [64] H. A. Bethe and E. E. Salpeter, *Quantum Mechanics of One- and Two-electron Atoms* (Plenum Publishing, New York, 1977).